Linwei Jiang[1], Baohua Ren[1], Cen Wang[1], and Chao Zhang[2]

[1] School of Earth and Space Sciences, University of Science and Technology of China, Hefei, China

[2] State Key Laboratory of Marine Environmental Science, College of Ocean and Earth Sciences, Xiamen University, Xiamen, China

Corresponding author: L.Jiang (jlw559@mail.ustc.edu.cn)

Key Points:

- The interannual variability of autumn precipitation in the central region of China is related to the second mode of the 200-hPa meridional wind field over the Eurasian continent (EC-a pattern).
- EOF2 features in '+-+' wave-like pattern, reinforces the southeasterly over the central region of China when it is in a positive phase.
- The local upward movement anomaly is largely dependent on the anomalous warm advection by the enhanced southerly pushing warmer air northward.
- Eurasian wave train could be excited by the North Atlantic dipole SST anomaly.

Abstract

The autumn precipitation in the central region of China (APCC) can exert great influences to the production and people's livelihood. With the use of reanalysis data from 1979−2020, we found a simultaneous relationship between the interannual variability of APCC and the second mode of the 200-hPa meridional wind field over the Eurasian continent, which featured a '+-+' wave-like pattern in autumn (denoted by EC-a). When EC-a is in a positive phase, the coupling of the positive geopotential height with anticyclonic anomalies in the upper level and low sea level pressure over the central China provides a conducive moisture and dynamic condition for precipitation, which is reversed in the negative phase. As indicated by the diagnostic equation, the local vertical motion anomaly is mainly dependent on the temperature advection anomaly by the perturbed wind acting on mean temperature. The strengthened anticyclonic wind shear over East Asia reinforces the southeasterly, which induces warmer air to move northward, resulting in a positive temperature advection and hence enhancing local ascending motion. Moreover, wave flux analysis and numerical simulations show that the EC-a wave train could be triggered by an abnormal dipole pattern SST over North Atlantic Ocean, which acts as a critical pacemaker on the variability of EC-a.

Keywords: autumn precipitation, Eurasian wave train, anticyclonic wind shear, North Atlantic dipole SST, interannual variability, model simulation

Plain Language Summary

The interannual variability of autumn precipitation in central region of China (APCC) is largely affected by a wave train over Eurasian continent (EC-a), which can influence the local moisture and dynamic uplift conditions by changing collocation of upper and lower flows. Furthermore, the North Atlantic dipole SST anomaly can serve as a crucial factor for predicting APCC, which excites the downstream EC-a wave train and is verified by numerical model.

1. Introduction

China is situated in a typical monsoon climate zone. Autumn is the transition period between the summer monsoon and winter monsoon, and because of this, autumn has different weather features than summer in terms of temperature and precipitation. The bimodal change in annual precipitation best describes the autumn rainfall in China. More than 20% of the local precipitation occurs in the areas with obvious autumn rain, which are primarily found in Sichuan, Chongqing, the Weishui and Hanshui River Basins, Eastern Yunnan, Guizhou, and other central regions. The autumn rainfall over western-central China, as the last stage of the rainy season over China, is a topic of particular interest and concern from ancient times to the present. Persistent rainy days and moderate precipitation amounts are the major characteristics of this area in the autumn season (Gao et al., 1958; Bai et al., 2004; Jiang et al., 2014).

Affected by its unusual geography, the central region of China is known for its intricate landscape, which includes mountains and foothills. Here, people are most closely clustered and rely on agriculture for a living. Since harvest and crop maturity occur in the autumn, the yield of crops in that year is directly impacted by the climate during this period. Changes in precipitation intensity can lead to floods and droughts that can jeopardize people's lives by reducing crop yields, causing landslides and other secondary disasters. Therefore, it is of great significance to study the climate in autumn for agricultural production and economic construction. (Bao et al., 2003; Peng et al., 2021; Wang et al., 2019). For instance, Shaanxi province had its wettest period, which broke the records since 1961, resulting in huge economic losses and casualty. Hence, in order to avoid the harm to the populace, it is necessary to understanding the mechanism of the variability of autumn precipitation in central region of China and increase its skillful predictability.

Previous studies have pointed out that the autumn rainfall in China is affected by the westerly jet and summer monsoon, and its important influence systems include the Western Pacific subtropical high, the India Myanmar trough, the Balkash Lake low trough, and the East Asian trough. (e.g., Bai et al., 2004; Jiang et al., 2014; Wang et al., 2019; Peng et al., 2021). In recent years, an increasing number of studies have found that the Eurasian wave train at mid-high latitudes in the northern hemisphere can affect the climate of East Asia via teleconnection.

There is evidence that in the extratropical zone, the monthly atmospheric circulation could regulate the atmospheric teleconnection formation, which is closely

associated with the local climate change. As reported by a number of studies, Eurasian wave trains are capable of affecting the weather and climate over the Eurasian continent from west to east, which has a significant impact on precipitation and temperature in China. (e.g., Hu et al., 2005; Ding et al., 2005, 2007; Chen et al., 2012; Liu et al., 2014). For instance, the Silk Road (SR) teleconnection, a dominant teleconnection pattern observed from the meridional wind field in the upper troposphere over the Eurasian continent, may affect the south-northward advance and retreat of the western Pacific subtropical high in summer, and thus affect the ending date and onset date of East Asian summer rainfall (e.g., Lu et al. 2002; Feng et al., 2013; Gong et al., 2013, 2015). Furthermore, Ding et al. (2005) reported that in the Northern Hemisphere, there is a boreal summer stationary circumglobal teleconnection (CGT) pattern, showing a zonal orientation similar to the Silk Road pattern, while exhibiting circumglobal characteristics. These researches indicated the high correlation of CGT with the summer monsoon system. As highlighted by Wang et al. (2014), the Eurasian teleconnection (EU) pattern might be a critical mid-tropospheric teleconnection pattern for the interannual variations in East Asian winter monsoon. As a main variability mode at low frequencies in the circulation of winter in the Northern Hemisphere, the EU teleconnection can lead to anomalies in the geopotential height (GPH) field over Eurasia, which modulate the precipitation and temperature anomalies in Eurasian region (Wang et al. 2015). These findings have largely improved the prediction of precipitation.

However, most of the studies concentrated on the impact of atmospheric teleconnection during summer or winter. The autumn season has rarely been investigated. Actually, the teleconnection patterns exhibit the features of seasonal change, possibly due to the weakness and poleward shift of the upper-level westerly jet stream. As reported by Terao et al. (1995) and Iwao et al. (2008), in addition to the widely investigated waveguide in subtropical regions with the propagation of the SRP or CGT, another waveguide is across the Eurasian continent within the polar front jet at higher latitudes, and both wave trains have significantly different effects on temperature and precipitation the climate along its route. As a seasonal shift, the Eurasian wave train in autumn presents one close to 45°-50° N at mid-high latitudes and the other close to 25°-30° N in the subtropical zone, and the northerly wave trains more significantly affect the temperature and precipitation in China (Guo et al., 2019). These researches suggested that the wave train could induce a low−pressure cyclonic circulation in Northeast China, resulting in an abnormally large amount of precipitation in the local region, while it shows a negative influence on the surface temperature and precipitation in Northwest China.

These results agree with Zhu et al. (2020), who found that the interannual variability in autumn rainfall in west-central China is closely related to the local horizontal trough, which is associated with a mid-high latitude barotropic Rossby wave train. In accordance with the definition of EU teleconnection, Xu et al. (2017) found a significant negative correlation between autumn rainfall in west China and the autumn EU index. During the positive anomaly phase

of the EU, the insufficient water vapor supply results in the recession of rainfall, while the negative anomaly phase indicates the opposite reaction. The EU index appears preferentially in autumn compared with any other atmospheric index. According to the above studies, the autumn Eurasian wave train patterns might have a connection with the precipitation and temperature in China in some way.

As the major forcing source for the upstream weather system of East Asia, many studies in recent years have focused on the effects of abnormal sea temperatures in the North Atlantic on weather and climate anomalies in China. It has been pointed out that the North Atlantic sea temperature anomaly can influence the atmospheric circulation in China by affecting the North Atlantic Oscillation. They suggested that atmospheric teleconnection might play an important role in bridging the Atlantic Ocean SST and the East Asia climate. Peng et al. (2021) indicated that the abnormal autumn rainfall in western China in 2017 was attributed to the combined effects of the anomalous warming of the Barents Sea SST and North Atlantic Ocean SST during the same time, with the equatorial Middle East Pacific SST in the La Nina pattern. (Xu et al., 2013) imply that the tripole SST anomaly pattern in the North Atlantic could excite a downstream Atlantic-Eurasian (AEA) teleconnection, which contributes to an increase early autumn (September) rainfall over Central China. Therefore, this paper will also discuss whether the related SST anomaly can affect the autumn precipitation in central China via atmospheric teleconnection, such as stimulating the Rossby wave train propagating eastward.

Thus, the paper is organized as follows. First, the features of the spatial and temporal variations in autumn rainfall in central China will be described. After that, we will investigate the teleconnection patterns over the Eurasian continent in autumn and determine whether a significant impact on the precipitation variations in central China exists. Furthermore, the excitation mechanisms of the associated atmospheric teleconnection will be clarified.

1. Data and Methods

(a) Data Sets

The central region of China is set as 27°–37° N, 100°–115° E, and autumn refers to the mean of September–October (SO) in this study. The data employed in this study are elucidated below:

1. The Global Precipitation Climatology Project monthly precipitation since 1979 integrating observations and satellite precipitation data is employed, with a 2.5° × 2.5° horizontal spatial resolution. (Adler et al., 2018)
2. The National Center for Atmospheric Research and the National Center for Environmental Prediction presented reanalysis data (M. Kanamitsu et al., 2002) of the global monthly mean GPH field, the air temperature field, the wind field (u, v components) and the specific humidity field. The atmospheric data have 2.5° × 2.5° horizontal spatial resolution and 17 isobaric surfaces from 1000 to 10 hPa vertically.

3. The NOAA Extended Reconstructed SST V5 provides the monthly mean SST data with a 2.0° × 2.0° horizontal resolution (Boyin H. et al. 2017);

   (a) Methods

To investigate the correlation between the two variables, regression analysis and composite analysis are used to promote this study, and the extreme events are excessive and insufficient years in accordance with their time series at ±0. 65 standard deviations. The t test suggests the two measurement sets' separateness. Accordingly, it is exploited for determining whether the two measurement sets are fundamentally different.

We diagnose the vertical motion anomaly based on the BASIC quasi-geostrophic omega equation:

$$(\nabla_P^2 + \frac{f^2}{\sigma}\frac{\partial^2}{\partial p^2})\omega = \frac{f_0}{\sigma}\frac{\partial}{\partial p}\left[\overrightarrow{v_g}\cdot\nabla_p\left(\xi_g + f\right)\right] + \frac{R}{\mathrm{p}}\nabla_P^2\left[\overrightarrow{v_g}\cdot\nabla_p T\right] \quad (1)$$

whereω denotes the vertical motion in pressure coordinates; $\overrightarrow{v_g}$ represents the geostrophic wind velocity vector; T expresses the air temperature, and ξ_g denotes the relative vorticity determined by geostrophic wind.

Here is the QG Omega equation from Bluesetein (1992) (Eq. 5.6.11) with the two primary forcing terms on the right-hand side of this equation. The meaning of the respective term is presented below:

Left Term: Local Vertical Motion; this term is proportional to –

The first term on the right-hand side (Term A): Change in Absolute Vorticity Advection with "Height"

The second term on the right-hand (Term B): Horizontal Temperature Advection

The small perturbation method (Peixoto JP. et al,1984) is used to investigate the cause of advection anomaly:

$$(\vec{v}\nabla T)^{'} = \overline{\vec{v}}\cdot\nabla T^{'} + \vec{v}^{'}\cdot\nabla\overline{T} + \vec{v}^{'}\cdot\nabla T^{'} \quad (2)$$

where the variables with bar and prime are their mean state and perturbation, respectively.

The propagation of anomalous Rossby waves is revealed by the method of Plumb (1985) (Eq. 4):

$$F_s = \frac{P}{P_0}\cos\varphi \times \begin{pmatrix} v'^2 - \frac{1}{2\Omega \mathrm{a}\sin 2\varphi}\frac{\partial\left(u'\Phi'\right)}{\partial\lambda} \\ u'v' + \frac{1}{2\Omega a\sin 2\varphi}\frac{\partial\left(u'\Phi'\right)}{\partial\lambda} \\ \frac{f}{S}\left[v'T' - \frac{1}{2\Omega a\sin 2\varphi}\frac{\partial\left(T'\Phi'\right)}{\partial\lambda}\right] \end{pmatrix} (2)$$

where a denotes Earth's radius; f expresses the Coriolis parameter; Φ represents the geopotential height (GPH); denotes the latitude;λ expresses the longitude;

represents the perturbation quantity; p_0 expresses pressure (1000 hPa); and F denotes the horizontal stationary wave activity flux (m^{-2}/s^{-2}).

To confirm the proposed mechanisms, numerical experiments based on the linear baroclinic model (LBM), developed by the Center for Climate System Research (CCSR) at the University of Tokyo and the National Institute for Environmental Studies (NIES) in Japan, are carried out.

The background state is prescribed as the autumn (SO) mean climatology during the period 1979–2020. The forcing in the model specifies the heat forcing, and we choose the dry conditions for further analysis in our study. The resolution of the LBM is triangular truncation of 21 waves (T21), corresponding to 5. 625° × 5. 625° in longitude and latitude with 20 vertical layers (L20) in the sigma coordinate (L20). The integration time of the model is set to 31 d because the atmospheric response usually reaches equilibrium at approximately 2 weeks. In this experiment, we will focus on the process of atmospheric responses to heat forcing by analyzing the geopotential height field of the model.

1. **Features of rainfall variations and atmosphere teleconnection patterns in autumn**

   (a) The rainfall variations in autumn and the corresponding atmospheric circulations

In this section, the spatial and temporal features of autumn precipitation variations in central China and the corresponding atmospheric circulations will be studied.

In autumn, more pluvial regions are used to appear in the central region of China. Fig. 1 (a) illustrates the spatial distribution of the climatological precipitation pattern in autumn from 1979 to 2020. As indicated by this figure, there exists a significant large value center in central China. Thus, we use the regional averaged precipitation over the domain of 27°–37° N, 100°–115° E in autumn as the rainfall index, as presented in the purplpe box.

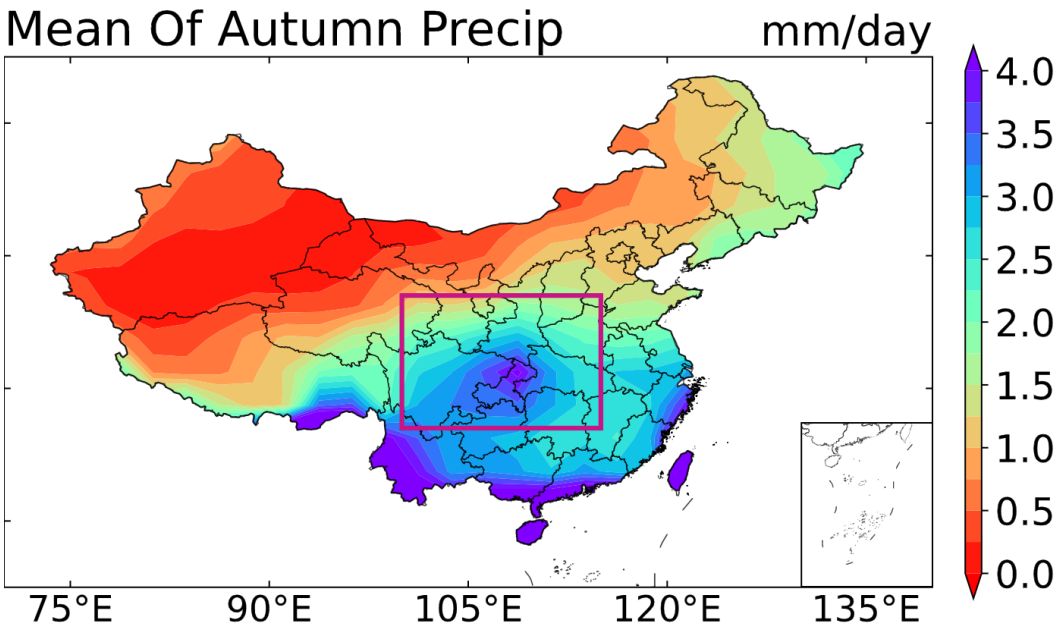

Figure 1. Mean precipitation in autumn (mm/day) during 1979–2020.

Since the Rossby wave train traveling along the jet stream in the mid-upper troposphere in the northern hemisphere is likely to have an effect on the north-western Pacific subtropical high's south-northward advancing and retreating in summer, thus affecting the ending date and onset date of the East Asian summer precipitation season (Ding et al., 2005; Feng et al., 2013; Gong et al., 2015), the following investigation is conducted on the 200-hPa circulation anomalies. As shown in Fig. 2 (a), from the correlation coefficients of the 200-hPa GPH anomaly field, a clear wave-like structure appears over the Eurasian continent propagating from west to east. Hence, one question raised is whether this spatial distribution is considered a typical pattern in autumn. If so, it could improve the predictability of autumn precipitation in the central region of China.

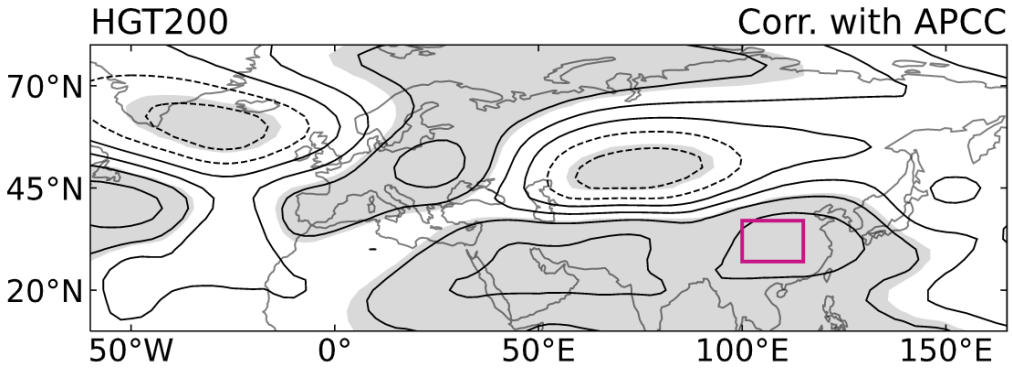

Figure 2. The correlation coefficients between autumn precipitation in the central region of China and 200-hPa geopotential height (by contours). The 95% confidence level is represented by shading.

1. Atmospheric teleconnection pattern in autumn and its relationship with precipitation

Interestingly, the atmospheric circulation anomaly corresponding to autumn rainfall in central China in Fig. 2(a) is in the form of a wave train pattern and highly resembles the SRP (Silk Road Pattern) teleconnection in summertime, which has an impact on the precipitation and temperature in East Asia. The SRP has a significant characteristic in that it travels longitudinally in the temperate zone with the Asian jet over Eurasia in the mid-upper troposphere, an anticyclone (cyclone) located in the Caspian Sea and the Korean Peninsula (the other 2 located in Eastern Europe and Mongolia) (Lu et al. 2002; Kosaka et al. 2009)

Thus, based on the empirical orthogonal function (EOF) method and the definition of the SRP by Kosaka et al. (2009), we analyzed the average meridional wind field at 200 hPa in 20°–60°N, 30°–130°E.

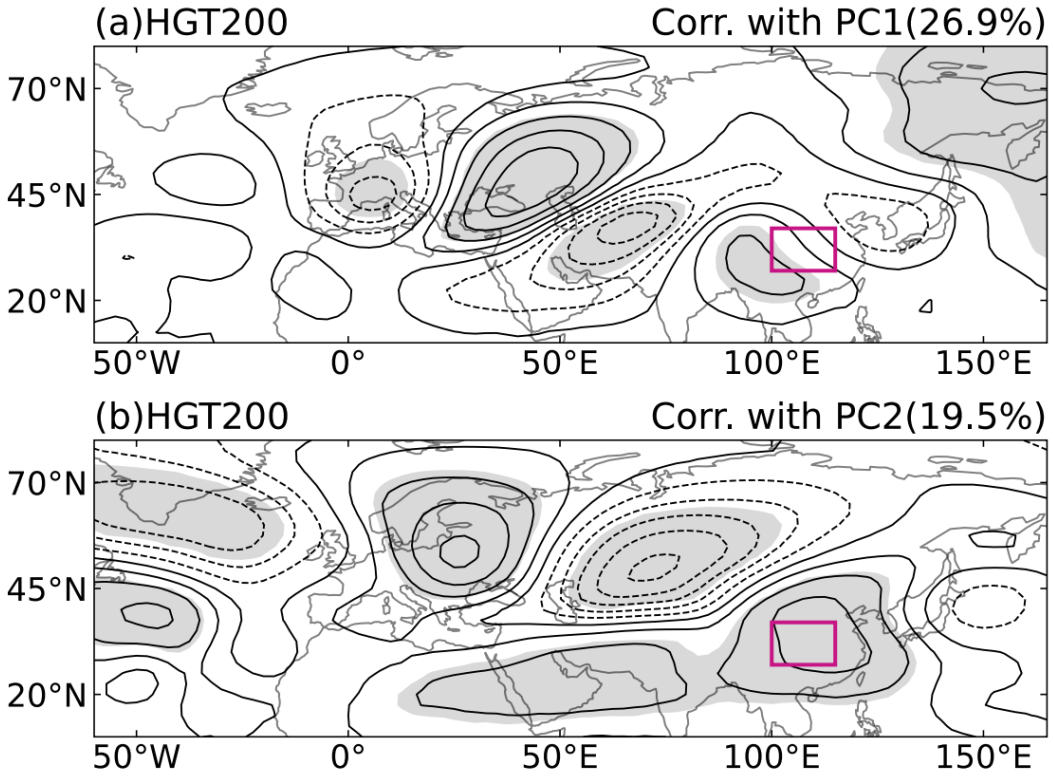

Figure 3. The correlation coefficients between PC1 (a) and PC2 (b) determined through EOF analysis on 200-hPa meridional wind velocity in 20°–60°N, 30°–130°E, and 200-hPa geopotential height (by contours) in autumn during 1979–2020. The 95% confidence level is represented by shading.

The variance fractions interpreted by the first two EOFs are 26.9% and 19.5%, respectively. These fractions can be separated from other modes. Because of the geostrophic balance at middle latitudes, the spatial patterns of the EOF analysis are presented as a correlation map of 200-hPa geopotential height anomalies. According to Fig. 3, there exist two different spatial patterns of wave trains over the middle to high latitudes. Specifically, the spatial distribution in Fig. 3(b) determined by EOF2 is consistent with the atmospheric circulation anomalies in Fig. 2(a), with a highly synchronous variation in the PC2 time series in Fig. 4(a) (r = 0.58, passing significance at 99%), thus revealing that EOF2 is significantly correlated with autumn precipitation in the central region of China. However, compared with EOF2, the correlations of precipitation with EOF1 are weaker(r=0.07) and do not pass the significance test at 90%, which is not shown. Therefore, the second mode of V200 over the Eurasian continent can be seen as a crucial factor affecting autumn precipitation over the central region of China. Since EOF2 exerts a closer link than EOF1, in the following analysis, we will only focus on the impact of the EOF2 pattern on the autumn precipitation in

the central region of China.

Considering that the South Asia High (SAH) is also prominent at the second mode of the meridional wind field and is related to East Asia monsoon rainfall (Bai et al., 2004; Wei et al., 2013), while this paper only focuses on the impact of Eurasian wave trains at mid-high latitudes, as a consequence, we further calculated the partial correlation coefficient after removing the SAH index to exclude the effect of the SAH. The partial correlation coefficient between Eurasian wave trains and autumn precipitation in central China is 0.51. Therefore, it can be considered that there is indeed a close link between Eurasian wave trains and autumn precipitation in central China, independent of the SAH.

The time series of the year-to-year intensity variation is shown in Fig 4(a). Both of these origin time series exhibit interdecadal variations, and the intensity experienced an interdecadal strengthening around the 2010s, which show consensus with other researchers (Wei et al., 2018, Zhu et al., 2020). However, we mainly focused on the relationship in the interannual variability between central China rainfall and Eurasian wave trains in autumn, and the interdecadal strengthening trend is not considered here. Thus, before discussing the impacts and mechanisms, the coherence on the interannual scale should be examined.

To separate the interannual variation from the interdecadal variation, the Butterworth highpass filter is employed (we also moved the linear trend). After filtering the original time series, the autumn precipitation in central China still correlates significantly with Eurasian wave trains with a correlation coefficient of 0.52 at the 99.9% confidence level, which indicates high coherence at the interannual timescale. Therefore, it is suggested that the relationship between the autumn precipitation in central China and Eurasian wave trains still maintains a high correlation after removing the long-term trend and interdecadal variations.

Hereafter, in following studies, the interannual component of PC2 is abbreviated as EC-a since this wave train propagates from Eurasia to China in autumn and the interannual component of autumn precipitation in central China is abbreviated as APCC.

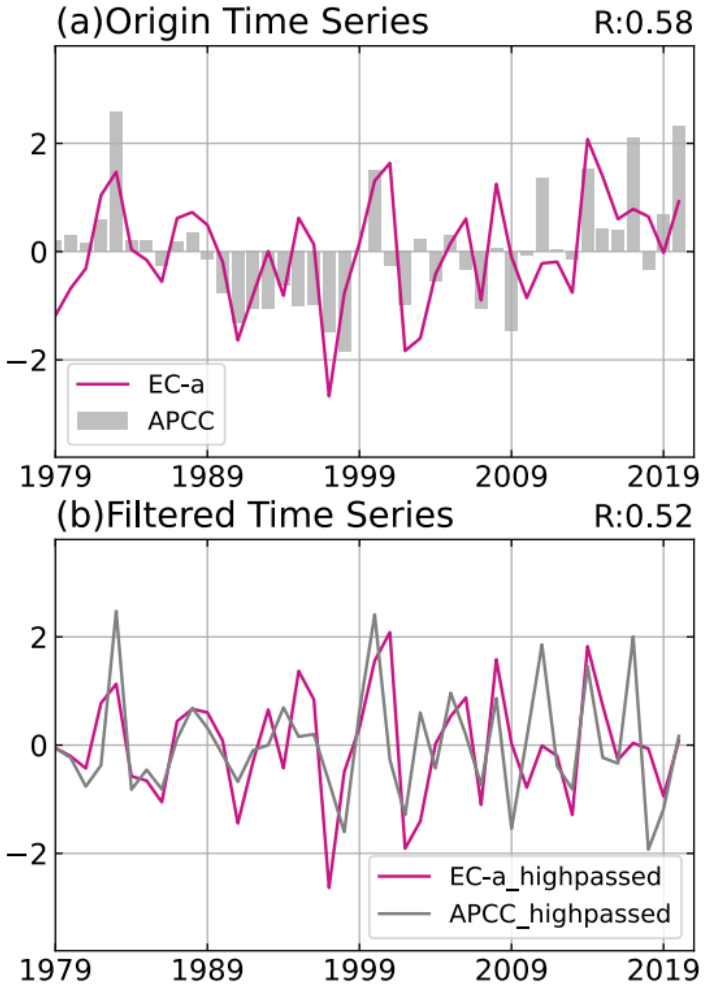

Figure 4. The origin time series of the year-to-year variability (a) and the filtered time series (b) of the interannual variability in APCC (purple) and EC-a (gray).

1. **Impact of the Eurasian wave train on autumn precipitation anomalies**

Fig. 5 demonstrates the atmospheric circulation responses in the troposphere to the EC-a anomalies by the spatial pattern of the zonal wind at 200 hPa, 500 hPa GPH, sea-level pressure (SLP) with the horizontal wind at 850 hPa, and the vertical profile of omega averaged over 27°N-37°N regressed on EC-a.

The 200 hPa zonal wind showed a weaken westerly wind anomaly near southern China, an abnormally strong westerly wind from the Caspian Sea across northern China up to Japan, and a center of subtropical westerly wind located

at Central Asia (20E-80E). The vast areas north of 27 °N are controlled by westerly wind anomalies, with the southerly region regulated by easterly wind anomalies. The central region of China is located at the southern side of the westerly jet, resulting in enhanced zonal wind shear, which corresponds to an anticyclone and negative relative vorticity. This abnormal distribution pattern provides favorable vertical motion conditions for precipitation.

Ding et al. (2005) indicated that when the center of the westerly wind jet in East Asia was moved from the west of the northwest Pacific to the northwest of the Tibetan Plateau, it was conducive to exciting Rossby waves propagating downstream along the Asian westerly wind flow, which exhibited positive GPH anomalies in East Asia. As verified in Fig. 3b, there was a significant abnormal distribution of the '+ - +' GPH in the upper troposphere during the positive phase of EC-a, with two positive anomaly centers over the Eastern European Plain and East Asian coast. A significant negative anomaly of GPH accounts for east of Ural to the west of Baikal Lake, thus leading to the southward movement of high latitude cold air. Meanwhile, the area of the Caspian Sea to Balkhash Lake is controlled by a relatively straight westerly wind, which reinforce the eastward transport of cold air from the high latitudes to China.

In the lower troposphere, significant anomalous southerly winds appear in the southern region of central China and turn to westerly winds with increasing latitude. The southerly winds transport water vapor from the South China Sea, and the westerly winds transport water vapor from the Pacific Ocean. Two flows converge over central China, resulting in the enhanced influx intensity of warm moist flow. Meanwhile, under the influence of the low-pressure system, a large supply of moisture is accumulated over central China, providing a favorable moist condition for precipitation.

Generally, the vertical velocity increased corresponding to increased precipitation. The vertical ascending movement transports the horizontally converged water vapor upward; at the same time, it makes the air adiabatically cool to saturation and then condenses into water drops to fall down. From the vertical profile of omega averaged over 27°N-37°N, the distribution of the vertical velocity corresponded well with the zone of precipitation. The pluvial region (110°E-115°E) is characterized by ascending movement, and the maximum value of the omega anomaly lies in the levels between 700 hPa and 200 hPa.

All the results indicate that the EC-a could influence the APCC by affecting the atmospheric circulation anomalies over the Eurasian region, leading to central China in the center of a low-pressure system in the low troposphere as well as the southwest edge of a high-pressure system in the mid-high troposphere. Impacted by the conjunctive actions of the abnormal circulation systems, the updraft is strengthened, and the excessive southeast moisture carried by this updraft is in turn favorable to the occurrence and development of rainfall.

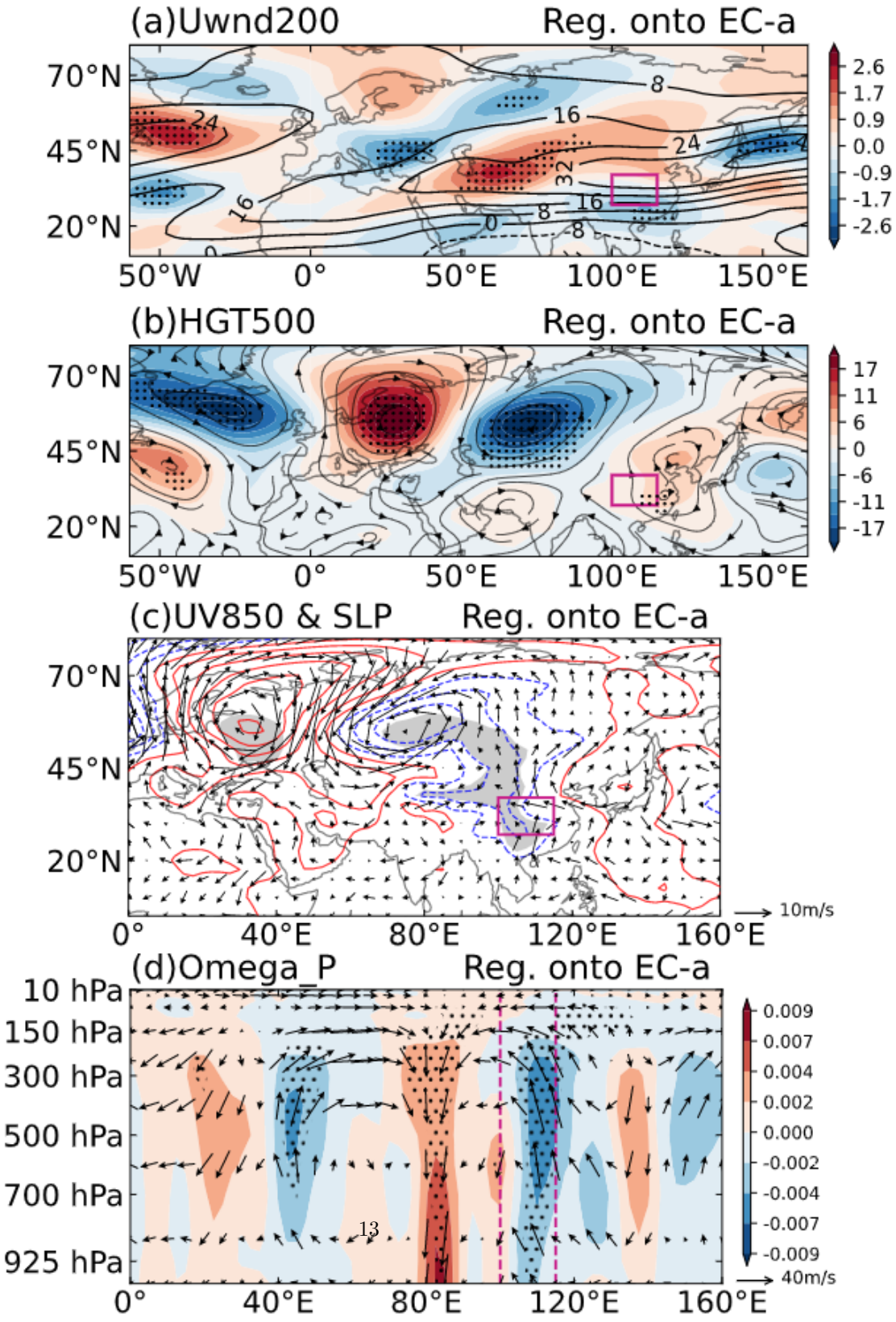
(a)Uwnd200
Reg. onto EC-a
70°N
45°N
20°N
50°W
0°
50°E
100°E
150°E
2.6
1.7
0.9
0.0
-0.9
-1.7
-2.6
(b)HGT500
Reg. onto EC-a
17
11
6
0
-6
-11
-17
(c)UV850 & SLP
Reg. onto EC-a
40°E
80°E
120°E
160°E
10m/s
(d)Omega_P
Reg. onto EC-a
10 hPa
150 hPa
300 hPa
500 hPa
700 hPa
925 hPa
0.009
0.007
0.004
0.002
0.000
-0.002
-0.004
-0.007
-0.009
40m/s

Figure 5. The regression map of zonal wind at 200 hPa and 500 hPa geopotential height (b), 850 hPa wind field and sea level pressure field (c) and height–longitude cross section of omega averaged over 27°-37°N (d) on the EC-a index for the same period. The 99% confidence level is represented by the dots and the gray shadows.

1. **Possible physical mechanism**

The abovementioned findings revealed that EC-a can be taken as a vital indicator for APCC by providing a favorable moisture and dynamic uplift condition. The possible physical mechanism for this close connection still needs to be explored in depth.

1. Diagnosis of moisture and dynamic uplift conditions

In this section, composite analysis is conducted to diagnose the moisture and dynamic uplift conditions. In our following analysis, the composite anomaly data are specified as the delta between positive and negative anomaly phases, unless otherwise stated. The positive and negative anomaly years are listed below:

Table 1. The anomaly years in positive EC-a phase and negative EC-a phase.

1979-2020	EC-a+	1982, 1983, 1988, 2000, 2001, 2008, 2014, 2015, 2017, 2020
	EC-a-	1979, 1991, 1992, 1994, 1997, 1998, 2002, 2003, 2007, 2010, 2013

The occurrence and maintenance of precipitation, especially heavy rainfall over a large area, is closely related to the presence or absence of sufficient water vapor transport to the relevant areas (Seager et al., 2010, Chou et al., 2013). Jiang et al. (2007) stated that the water vapor, which affects precipitation in the west region of China, is mainly derived from the Qinghai Tibetan Plateau, the Bay of Bengal, and the South China Sea. Therefore, the water vapor flux and divergence associated with abnormal precipitation in the central region of China need to be analyzed. When calculating the water vapor flux of the whole layer, considering that the moisture content in the atmosphere and the water vapor transportation are mainly below 300 hPa (Zhou et al., 2003), the integration of the water vapor flux is only calculated from the surface to the upper 300 hPa.

As seen from the composite difference in vertically integrated water vapor flux (Fig. 6a), the anomalous anticyclonic wind shear over the coast of East Asia reinforces southeast water vapor transport, facilitating warm and wet moisture from the South China Sea and the West Pacific to gather in the central region of China.

It can also be seen from the anomalous distribution of water vapor flux divergence (Fig. 6b) that significant water vapor flux convergence exists in most areas of the central region of China except for the areas in the northeast. At the same time, under the enhanced westerly wind, the cold air at mid-high latitudes

penetrates continuously from the west, while the central China is between the anomalous cyclone and anomalous anticyclone, becoming the intersection area of dry and cold flows and warm and wet air flows, which provides a favorable moisture condition for the development of local precipitation.

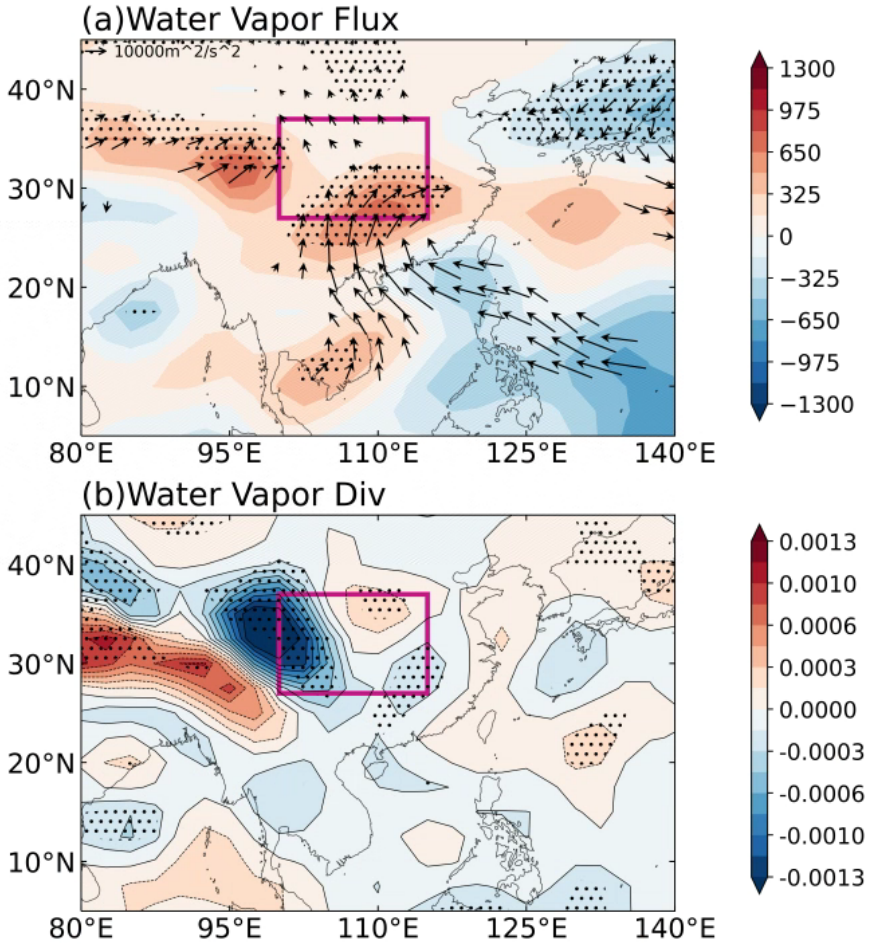

Figure 6. Composite water vapor flux (a) and divergence of water vapor flux (b) integrated from the surface to the upper 300 hPa between the positive and negative phases of the EC-a. The 90% confidence level is represented by the dots.

The convergence of water vapor flux is mainly determined by the horizontal convergence of air and thus coupled to conditions of vertical motion. Therefore, the local vertical motion anomaly is diagnosed by the BASIC quasi-geostrophic omega equation (Eq. 1). According to Fig. 7, term B displays a similar pattern as the omega anomaly displayed in Fig. 6 with a significant anomalous center over the central region of China. However, term A is significantly negatively

correlated with the local vertical motion anomaly, and the magnitude of term B is higher than that of term A. From the results of the diagnostic equation, temperature advection is the positive contribution, while absolute vorticity advection is the opposite. Thus, we conclude that when central China is in the pluvial period, the temperature advection anomaly accounts for the dominant status in local vertical motion anomaly in the mid-high troposphere, inducing a change in APCC.

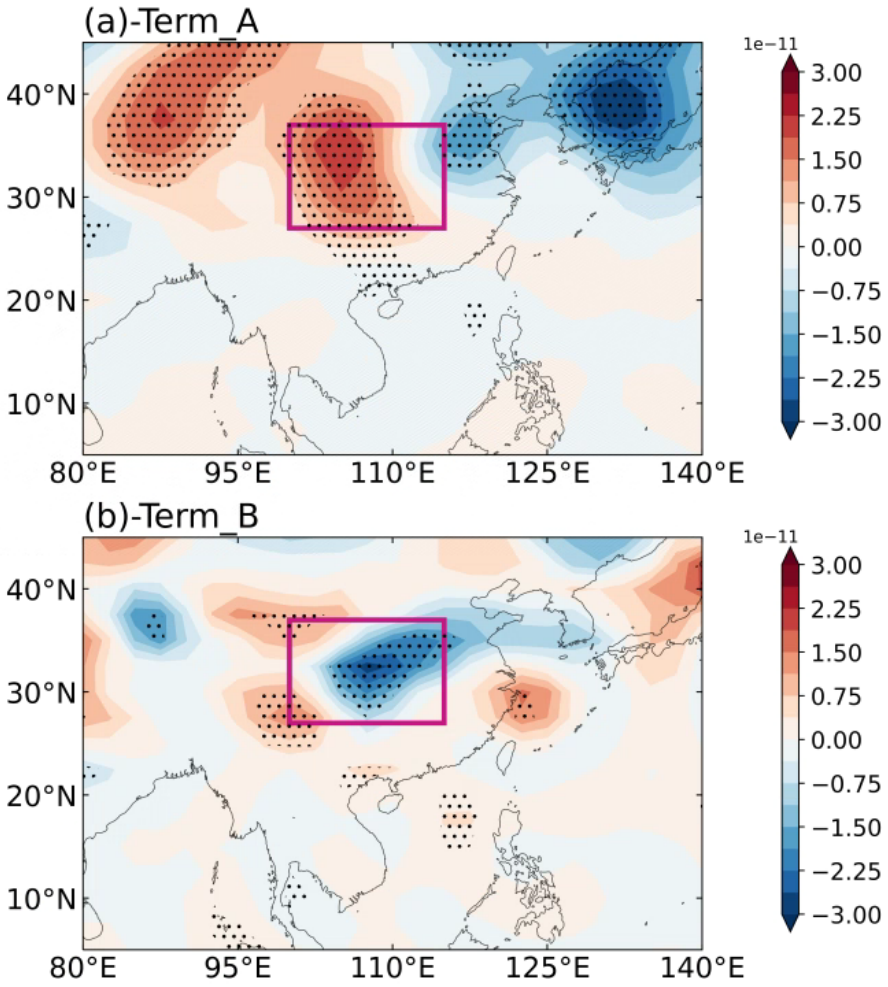

Figure 7. Composite term A (a) anomalies and term B (b) anomalies averaged at 300-700 hPa between the positive and negative phases of the EC-a. The 90% confidence level is represented by the dots.

To explore what makes the local term B of temperature advection vary in different EC-a phases, we use the small perturbation method to divide it into three terms (as denoted by Tadv1-3) according to analysis of the quasi-geostrophic

omega equation in Wei et al., (2013) (Eq.4b), which is written as:

$$\frac{R}{\mathrm{p}}\nabla_P^2\left[\overrightarrow{v_g}\cdot\nabla_p T\right] = \frac{R}{\mathrm{p}}\nabla_P^2[\overline{\overrightarrow{v_g}}\cdot\nabla_p T' + \overrightarrow{v_g}'\cdot\nabla_p\overline{T} + \overrightarrow{v_g}'\cdot\nabla_p T'] \quad (3)$$

Where – represents the mean stage, represents the perturbation quantity, respectively. And we compare the magnitude of the three terms to determine the main contributors to the temperature advection anomaly over central China.

Since the anomalous ascending motion is more significant in the mid-high troposphere (300 hPa-700 hPa), it is suitable to calculate these layers respectively. According to Fig. 8a, all layers show that the temperature advection anomaly primarily arises from the advection of perturbed wind field acting on mean temperature field. Additionally, the results at the respective level in the mid-high troposphere display a high similarity, which emphasize the effect of the perturbed southeast wind under the climatological-mean background of cold air in the north and warm air in the south, resulting in temperature advection anomaly over central China.

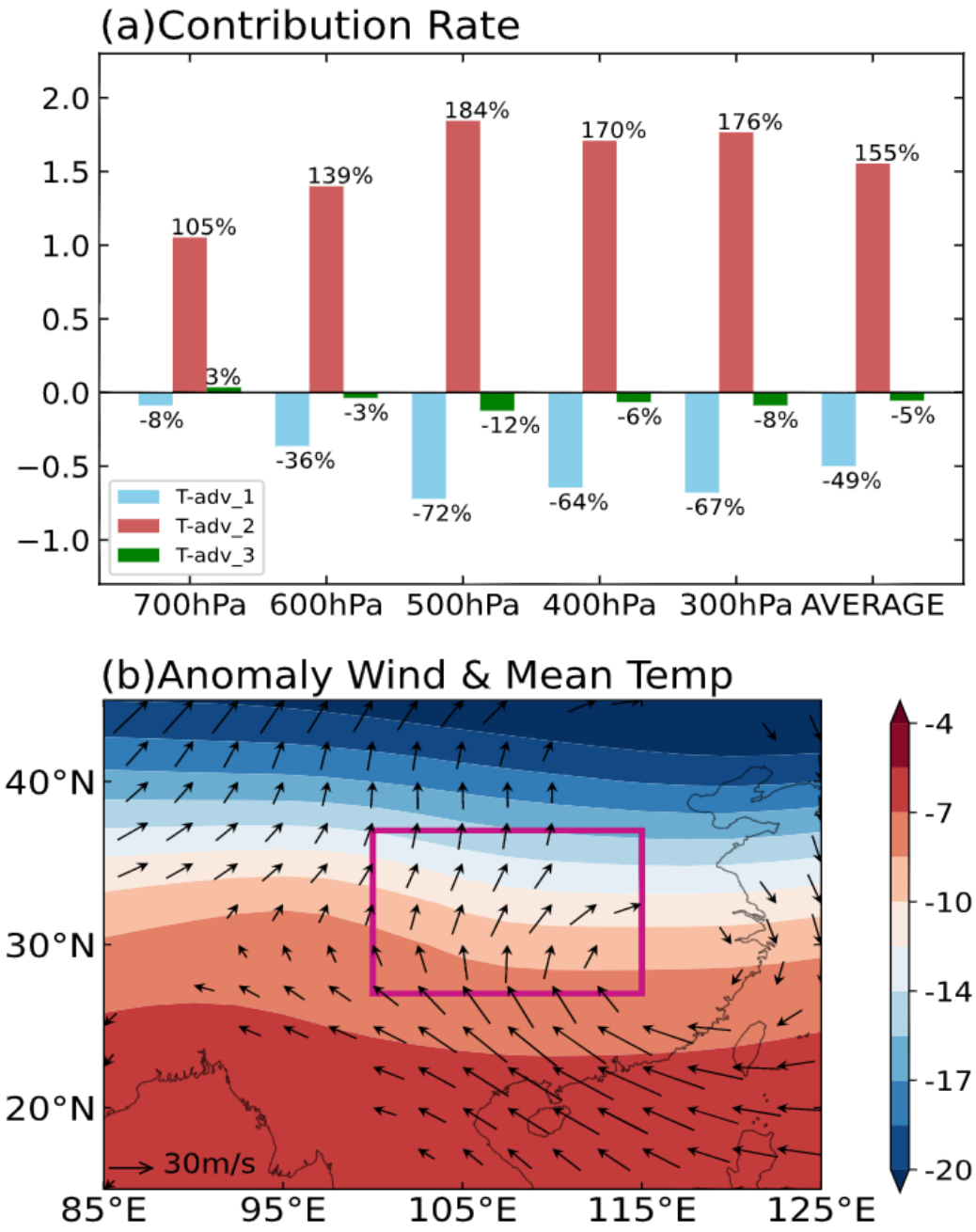

Figure 8. Contribution rate (a) of 3 terms on composite temperature advection anomalies between the positive and negative phases of the EC-a at 300-700 hPa averaged over the central region of China (27°–37°N, 100°–115°E), denoted by

T-adv1 (blue), T-adv2 (red), and T-adv3 (green). (b) The mean temperature and the perturbed wind responding to the EC-a anomaly averaged at 300-700 hPa (black vectors, passed the 95% confidence level)

In fact, it agrees well with the anomalous atmospheric circulations presented in Fig. 5(b). To better illustrate the mechanism, we show the mean temperature and the perturbed wind averaged at 300-700 hPa (Fig. 8b). In the positive EC-a phases, the East Asian coast is mainly dominated by an abnormal anticyclone, thus bringing rise to an anomalous southeast wind over the central region of China and inducing warmer air to move northward, resulting in a positive temperature advection anomaly. Thus, warm air advection in the mid-high troposphere can lead to more significant upward motion over the central region of China.

1. The wave source of the EC-a teleconnection pattern

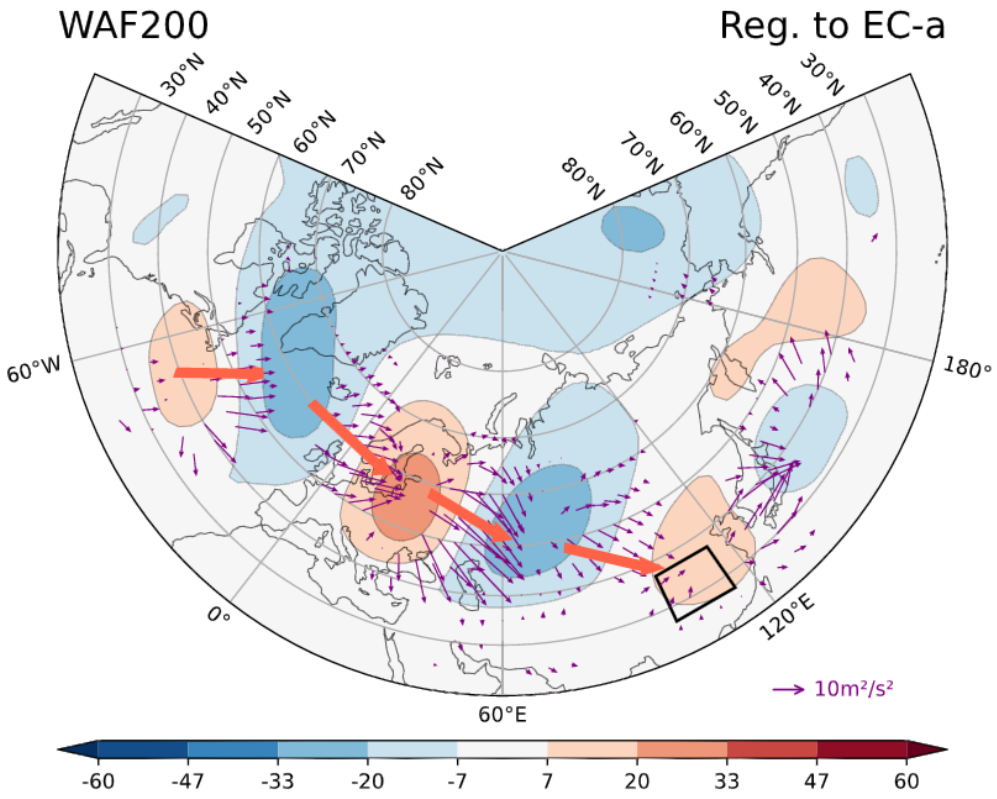

Figure 9. The regression map of the wave activity flux (m^2/s^2) (vectors, passed the 95% confidence level) and the geopotential height (shading contours) at 200 hPa on the EC-a index.

To better understand the EC-a pattern wave train and improve the predictability

of APCC, the source of this wave train should be clarified.

Wave flux is a measure of wave energy transmission and can be used to diagnose wave propagation and wave-flow interactions (Plumb, 1985). Therefore, the horizontal component of wave flux is employed to discuss the propagation characteristics of Rossby wave energy, and the zonal and meridional components of wave action flux are calculated.

As demonstrated by the associated wave fluxes (Fig. 9), in accordance with the distribution of anomalous atmospheric circulation, the average horizontal wave flux at 200 hPa converges and diverges over the North Atlantic, and the wave vector is basically eastward in the zonal direction. During the process of wave propagation in the east, the transmission direction of the wave flux gradually shifts southward in Central Asia. Specifically, the Rossby wave flux originating from North Atlantic Ocean propagates from west to the east across Europe and Siberia and finally converges into a positive GPH with an anomalous anticyclone over the coast of East Asia, and the central China is located southwest edge of this system. Affected by the anomalous anticyclonic wind shear, the southeasterly wind is intensified, pushing a plenty of warm and moist air to central China and forming a warm air advection anomaly, which can further induce the change in APCC.

As the main forcing source of the upstream weather system in China, there has been a great deal of research in recent years on the influence of abnormal sea surface temperature (SST) forcing in the North Atlantic on East Asian climate anomalies. Zhang et al. (2018) pointed out that the North Atlantic SST anomalies in spring are the most significant forcing signal for the phase variation of Rossby waves in the Eurasian continent. Du et al. (2020) suggested that the anomaly of the North Atlantic SST can affect the atmospheric circulation in China by affecting the North Atlantic Oscillation. When the North Atlantic SST anomaly presents a '+-+ 'phase, a teleconnection wave train propagating over Eurasian continents at mid-high latitudes can be triggered, which causes a positive anomaly of Ural blocking high, thus resulting in the late start of the rainfall and a large amount of precipitation in the Yangtze River (Zuo et al., 2013). The abnormal warming of the North Atlantic will strengthen the Siberian high ridge and benefit the southward movement of cold air, which is closely related to the large-scale cold and frozen disaster weather in southern China in January 2008 (Zong et al., 2008).

Combined with the aforementioned abnormal wave fluxes over the North Atlantic, we infer that the Rossby wave source lies in this region and the temperature anomaly in North Atlantic Ocean may excite the EC-a wave train, thus affecting precipitation in the central region of China. First of all, the linear correlation between EC-a index and global SST field is analyzed to observe whether there is association between EC-a and the North Atlantic SST. When EC-a is anomaly, there is no obvious SST anomaly in the tropical Pacific and Indian Ocean, while an anomalous distribution pattern of the north-cold (50°- 65°N 20°- 50°W) and south-warm (25°- 50°N 40°- 70°W) dipole SST exists over

the North Atlantic.

Hereafter, we define these two regions as North Atlantic Ocean temperature critical regions and the critical region SST anomalies may further influence the autumn precipitation in central region of China by exciting the Rossby wave train as the EC-a teleconnection pattern.

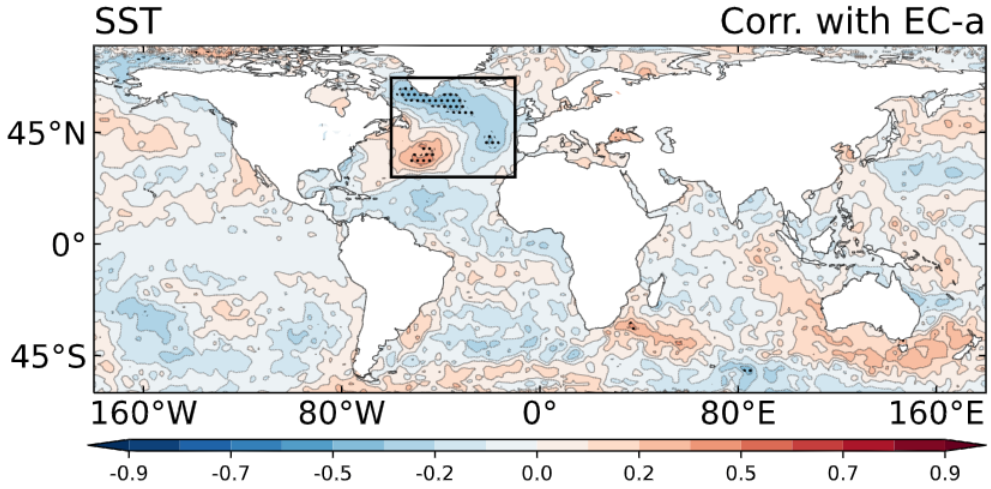

Figure 10. The correlation coefficients between EC-a index and sea surface temperature. The 95% confidence level is represented by the dots.

To verify this conjecture, the linear baroclinic model (LBM) is used to simulate the forcing effect of the dipole SST anomaly in North Atlantic Ocean. By using the LBM, Watanabe et al. (2000) simulated atmospheric responses to the heat source located in the central North Atlantic and discussed the relative contributions of sensible heat and latent heat to the formation of the North Atlantic Oscillation (NAO). Qiu et al. (2014) used LBM to simulate the middle latitude atmospheric response to heat and vorticity forcing and soon compared the influence of variability in Indian summer mon on the East Asian summer monsoon. Hence, in our sensitivity experiment, the cold and warm sea surface air temperature forcing is added in two key areas.

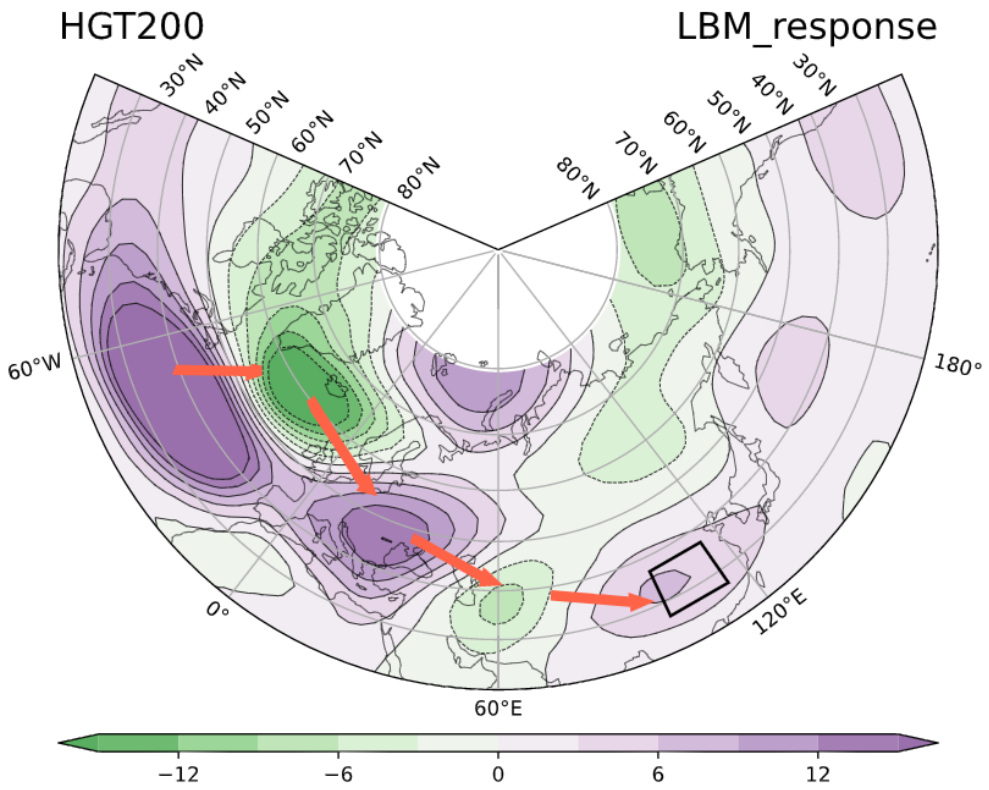

Figure 11. The 200 hPa geopotential height response to the North Atlantic sea surface air temperature forcing in the LBM model.

From the present GPH anomaly simulated by the model, the model can simulate similar autumn Eurasian wave trains. As shown in Fig. 11(b), there are meridional positive and negative geopotential height anomalies over the North Atlantic, positive GPH anomalies with anticyclones over the European Plain and the coast of East Asia, and negative GPH height anomalies with cyclones in Central Asia, showing the characteristics of Eurasian wave trains as a whole. From the model simulation results, it can be seen that the wave train excited by the North Atlantic dipole SST pattern over North Atlantic Ocean via Eurasia to East Asia roughly matches the EC-a wave train in autumn. Therefore, the North Atlantic dipole SST anomaly plays a critical role in the formation of wave trains over Eurasia in the Northern Hemisphere in autumn, thereby affecting the precipitation in central China.

1. Conclusions

Using the NCEP/NCAR reanalysis atmospheric data and precipitation data, a wave train over the Eurasian continent is found by the empirical orthogonal function (EOF) method in the September-October meridional wind at 200 hPa

during the period 1979-2020, which shows a considerably high degree of positive correlation (r=0.52, with the 99% confidence level) with autumn precipitation over the central region of China at the interannual timescale. This middle latitude atmospheric teleconnection in the Northern Hemisphere can present more insights into the local precipitation in autumn and improve the skills of prediction further.

As revealed by the regression analysis, when EC-a is in a positive phase, a "+-+" atmospheric circulation pattern from Europe to China at 20° ~ 60°N exists in the mid-high troposphere. The wave train forms a positive GPH anomaly as well as an anomalous anticyclone along the East Asian coast, and the central region of China is located southwest of the anomalous center. In the lower troposphere, the central region of China is dominated by a negative SLP with the southeast wind anomaly, which facilitates the transport and convergence of water vapor. And the results are reversed in the negative phase.

In order to investigate the physical mechanism, the research also does the diagnosis analysis. By the diagnosis of water vapor flux, there is a water vapor transmitting belt from the Northwest Pacific to the central region of China. The anomalous anticyclonic circulation reinforces southeasterly, facilitating the water vapor transport and accumulation. Additionally, the analysis of QG-Omega equation indicates that the vertical motion anomaly is significantly related to the temperature advection anomaly, which is attributed by the perturbed wind field acting on the mean temperature field. The anomalous southeasterly strengthens the warm advection, leading to the upward movement enhanced.

In this paper, we aim to improve the predictability of APCC, by exploring EC-a teleconnection. Thus, it is necessary to figure out the source of this wave train. From the diagnosis of Plumb wave flux, one of the major forcing sources of the EC-a may be the abnormal dipole pattern SST over North Atlantic Ocean. Furthermore, the simulation of LBM confirms the key physical process linking the SST over North Atlantic Ocean with APCC via the EC-a. When the distribution of SST is cold in the north (50°- 65°N 20°- 50°W) and warm in the south (25°- 50°N 40°- 70°W) dipole pattern, the Rossby wave train could be triggered, which induces the positive GPH (anticyclonic) anomaly in the upper troposphere over the coast of East Asia, resulting in heavier autumn rainfall over central China.

The physical process can be summarized below (Fig. 12). The atmospheric circulation anomaly is triggered by abnormal dipole SST over North Atlantic Ocean, propagating downstream across the Eurasian continent via Rossby waves. After the wave trains spread to the coast of East Asia, a positive GPH anomaly is formed with the anomalous anticyclone wind shear, leading to a strengthened southeasterly, which reinforces the ascending motion by the effect of the warm advection and enhances southeasterly water vapor transport to central China. Hence, a sufficient moisture condition and an uplifting dynamic condition for excessive APCC are

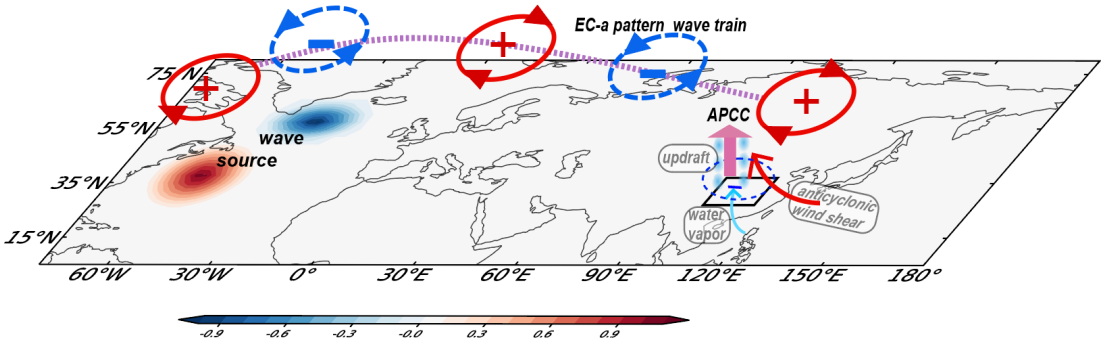

formed.

Figure 12. Schematic diagram of the physical process.

Open Research

The LBM model is available at https://ccsr.aori.u-tokyo.ac.jp/~lbm/., provide by the Center for Climate System Research (CCSR) at the University of Tokyo. The research data is available at https://psl.noaa.gov/data/., provide by the Physical Sciences Laboratory at the National Oceanic and Atmospheric Administration (NOAA).

References

Adler, R. F., M. Sapiano, (2018), The Global Precipitation Climatology Project (GPCP) Monthly Analysis (New Version 2.3) and a Review of 2017 Global Precipitation. Atmosphere, 9(4), 138, doi:10.3390/atmos9040138.

Bai H., Dong W. (2004), Climate features and formation causes of autumn rain over southwest China, *Chin. J. Plateau Meteor.*, 23(6),884–889

Bao Y., Ablmit LF., Wang X. (2003), Space-time distribution and physical mechanisms of autumn rains in west China in 2001, *J. Appl Meteor Sci.*, 14,215–222

Bluestein, H. B., (1992), Principles of Kinematics and Dynamics, *Oxford University Press*, *Synoptic-Dynamic Meteorology in Midlatitudes,* Vol. I, 431 pp.

Boyin H., Peter W., (2017), NOAA Extended Reconstructed Sea Surface Temperature (ERSST), Version 5. doi:10.7289/V5T72FNM.

Chen TC., Wang SY., Huang WR., Yen MC (2004), Variation of East Asian summer monsoon rainfall, *J. Clim.*, 17,2271–2290

Chou, C., Chiang, J., Lan, (2013), Increase in the range between wet and dry season precipitation, *Nature Geosci*, 6, 263-267, https://doi.org/10.1038/ngeo1744.

Ding Q., Wang B. (2005), Circumglobal teleconnection in the Northern Hemisphere Summer, *J. Clim.*,18,3483–3505

Ding Q., Wang B. (2007), Intraseasonal teleconnection between the summer Eurasian wave train and the Indian Monsoon, *J. Clim,*, 20, 3751–3767

Du Y., Zhang J., Zhao S., Chen H. (2020), Impact of Eastward shift in the negative-phase NAO on extreme drought over northern China in summer, *J. Geophys. Res.*, 125,16, https://doi.org/10.1029/2019JD032019

Ehsan, M.A., Nicolì, D., Kucharski (2020), Atlantic Ocean influence on Middle East summer surface air temperature, *NPJ. Clim. Atmos. Sci.*, 3, 5. https://doi.org/10.1038/s41612-020-0109-1

Feng G., Zhao J., Zhi R., Gong Z. (2013), Recent progress on the objective and quantifiable forecast of summer precipitation based on dynamical statistical method, *J. Appl. Meteorol. Sci.*, 24,656–665

Gao Y., Guo Q. (1958), On the autumn raining area in China, *Acta Meteor Sin.*, 29(4), 264–273

Gong Z., Feng G., Ren F., Li J. (2013), A regional extreme low-temperature event and its main atmospheric contributing factors, *Theor. Appl. Climatol.*, 117,195–206

Gong Z., Feng T., Fang Y. (2015), Objective identification research on cold vortex and mid-summer rainy periods in Northeast China, *Chin. Phys. B.*, 24,049204

Guo Y., Tian M., Chen Y. (2019), Influence of autumn Eurasian wave train on precipitation and surface temperature of China, *Yunnan University. J. Natural Sci.,* 41(4), 746-752

Hu K., Huang G., Wu R., (2018), Structure and dynamics of a wave train along the wintertime Asian jet and its impact on East Asian climate, *Clim. Dyn.*, 51, 4123–4137, https://doi.org/10.1007/s00382-017-3674-1

Iwao K., M. Takahashi, (2008), A precipitation seesaw mode between northeast Asia and Siberia in summer caused by Rossby waves over the Eurasian continent, *J. Clim.*, 21, 2401–2419, https://doi.org/10.1175/2007JCLI1949.1.

Jiang Z., Z. Ma., J. Liu., (2014), A study of improved index and climatological characters of autumn rain in western China, *Chin. J. Atmos. Sci.*, 38, 32–44.

Jiang X, Li Y, Li C., (2007), Characteristics of summer water vapor transportation in Sichuan basin and its relationship with regional drought and flood, *Chin. J. Plateau Meteor.*, 26 (3), 476–484.

Kosaka Y., Nakamura H., Watanabe M., (2009), Analysis on the dynamics of a wave−like teleconnection pattern along the summertime Asian jet based on a reanalysis dataset and climate model simulations (Evaluations of CMIP3 model performance for various atmospheric and oceanic phenomena, part I), *J. Meteor. Soc. Japan.,* 87,3, 561-580

Liu Y., Wang L., Zhou W., Chen W. (2014), Three Eurasian teleconnection patterns: spatial structures, temporal variability, and associated winter climate anomalies, *Clim. Dyn.*, 42,2817–2839

Lu R., J. Oh., B. Kim, (2002), A teleconnection pattern in upper-level meridional wind over the North African and Eurasian continent in summer, *Tellus*, 54A, 44–55, https://doi.org/10.3402/tellusa.v54i1.12122.

M. Kanamitsu, W. Ebisuzaki,(2002), NCEP-DOE AMIP-II Reanalysis (R-2), Bulletin of the American Meteorological Society., 1631-1643.

Peixoto JP., Oort AH., (1984), Physics of climate, *Rev Mod Phys.*,56,365–429

Peng Y., Xu H., (2021), Circulation features and causes of the anomalous rainfall over the West China in 2017, *Chin. J. Meteor Sci.*, 41(3), 363-373

Plumb A., (1985), On the three-dimensional propagation of stationary waves. *J Atmos Sci.*, 42(3), 217-229.

Qiu S., Fang J., Yang X., (2014), Mid-latitude atmospheric responses to heat and vorticity forcing using a linear baroclinic model, *Chin. J. Meteor Sci.*, 34(2), 149-161.

Seager R., Naik N., Vecchi G. A., (2010), Thermodynamic and Dynamic Mechanisms for Large-Scale Changes in the Hydrological Cycle in Response to Global Warming, *J. Clim*, 23(17), 4651-4668. https://doi.org/10.1175/2010JCLI3655.1

Terao, T., (1998), Barotropic disturbances on intraseasonal time scales observed in the midlatitudes over the Eurasian continent during the northern summer. *J. Meteor. Soc. Japan.*, 76, 419–436.

Watanabe M., Kimoto M., (2000), Atmosphere-ocean thermal coupling in the North Atlantic: a positive feedback., *Quart. J. Roy. Meteor. Soc.*, 126, 3343-3369

Wang L., Chen W. (2014), An intensity index for East Asian winter monsoon, *J. Clim.*, 27, 2361–2374. https://doi.org/10.1175/JCLI-D-13-00086.1

Wang N., Zhang Y., (2015), Evolution of Eurasian teleconnection pattern and its relationship to climate anomalies in China, *Clim.Dyn.*, 44, 1017–1028, https://doi.org/10.1007/s00382-014-2171-z

Wang Z., B. Zhou, (2019), Observed decadal transition in trend of autumn rainfall over Central China in the late 1990s, *J. Clim.*, 32, 1395–1409, https://doi.org/10.1175/JCLI-D-18-0112.1.

Wei W., Ren Z., Min W., (2013), Impact of Indian summer monsoon on the South Asian High and its influence on summer rainfall over China, *Clim.Dyn.*, 43, 1257-1269, https://doi.org/10.1007/s00382-013-1938-y.

Wei, T., He S., Yan Q., Dong W., Wen X. (2018), Decadal Shift in West China Autumn Precipitation and its Association with Sea Surface Temperature, *J. Geophys. Res.*, 123, 835-847, https://doi.org/10.1002/2017jd027092.

Xu J., Yan C., Zhong Y., (2017), Relationships between Eurasian Teleconnection Pattern in Northern Hemisphere Autumn and Autumn rainfall in West China, *Chin. J. Meteor. Sci. Tech.*, 45(3), 492~498

Xu H., Feng J., Sun C., (2013), Impact of Preceding Summer North Atlantic Oscillation on Early Autumn Precipitation over Central China, *Atmos. Ocean. Sci. Lett.*, 6, 417-422, DOI: 10.3878/j.issn.1674-2834.13.0027

Zhang Q., Xuan S., Sun S., (2018), Anomalous Circulation Characteristics of Intraseasonal Variation of East Asian Subtropical Westerly Jet in Summer and Precursory Signals, *Chin. J. Atmos. Sci.*, 42(4): 935-950. doi: 10.3878/j.issn.1006-9895.1803.18107

Zhou B., (2013), Weakening of winter North Atlantic Oscillation signal in spring precipitation over southern China, *Atmos. Ocean. Sci. Lett.*, 6, 248–252, https://doi.org/10.1080/16742834.2013.11447089.

Zhu Z., (2020), Dynamic Origin of the Interannual Variability of West China Autumn Rainfall, *J. Clim.*, 33, 9643-9652, https://doi.org/10.1175/jcli-d-20-0097.1.

Zong H., Zhang Q., Bueh C., (2008), Numerical Simulation of Possible Impacts of Kuroshio and North Atlantic Sea Surface Temperature Anomalies on the South China Snow Disaster in January, *Clim. Env. Res.*, 13(4), 491-499. doi: 10.3878/j.issn.1006-9585.2008.04.13

Zuo J., Li W., Sun C., (2013), Impact of the North Atlantic sea surface temperature tripole on the East Asian summer monsoon, *Adv. Atmos. Sci.*, 30(4): 1173-1186.